RSC Advances

ROYAL SOCIETY OF CHEMISTRY

www.rsc.org/advances

Performance of Novel Ag-n-TiO_2/PVC Reinforced Hollow Fiber Membrane Applied in Water Purification: *In-Situ* Antibacterial Property and Resistance to Biofouling

Zhenjiang Yu [a,b], Yuanyuan Zhao [a], Bing Gao [c], Xuyang Liu [d], Liming Jia [e], Fangbo Zhao [a,b,*], Jun Ma [b]

[a] School of Material Science and Chemical Engineering, Harbin Engineering University, Harbin, China, 150001

[b] State Key Laboratory of Urban Water Resource and Environment, Harbin Institute of Technology, Harbin, China, 150090

[c] Shanxi Telecommunications Planning and Designing Institute Co Ltd

[d] Ascend Performance Materials LLC, FM 2917 Rd, Alvin, TX 77512,USA

[e] Environmental Monitoring Centre Of Heilongjiang Province, Harbin, China, 150056

* Correspondent author. Tel: +8615114587583; E-mail address: zfbhit@163.com

Abstract

To improve the anti-biofouling properties of the membranes, Ag-embedding nano-sized titanium dioxide (Ag-n-TiO_2) particles were utilized as the biocidal agents to modify polyvinyl chloride (PVC) membranes. Both the Ag-n-TiO_2/PVC flat sheet membranes and reinforced hollow fiber membranes were fabricated by phase inversion method with varying Ag-n-TiO_2 particles concentrations. As a result, the hydrophilicity, permeability, and retention capability increased with Ag-n-TiO_2 concentration from 0 to 1.5 wt%. In addition, the in-situ antibacterial and anti-formation of biofilm properties of the modified membranes were greatly enhanced in conventional inhibition zone test, *Escherichia coli* (*E. coli*) absorption experiment, fluorescence stain, as well as long-term continuous biofouling test. The best results were obtained for PVC membrane modified by 1.0 wt% Ag-n-TiO_2. The optimized membrane presented not only better permeability and in-situ antibacterial property in *E. coli* adhesion, but also the enhancement in resisting biofilm formation and more steady permeation flux in the long-term filtration than the unmodified membrane.

Keywords: Ag-n-TiO_2 nanoparticle; Polyvinylchloride (PVC); In-Situ Antibacterial; Anti-biofouling; Reinforced hollow fiber membrane

1. Introduction

Ultrafiltration (UF) has been widely used as a simple and convenient process for water and wastewater treatment regarding its relatively low cost and high separation efficiency [1-3]. However, membrane fouling reduces the performance as well as process economics and hence, restricts its widespread applicability [4-6]. Several types of membrane fouling have been identified currently, including inorganic fouling, organic fouling, and biofouling [7-10]. Among them, biofouling is a persistent, dynamic, and complex process [11-16]. Once biofouling occurs in the membrane systems, there is no effective method to mitigate the fouling, and membrane replacement has to be conducted [13].

To control biofouling, some strategies have been studied, such as feed pretreatment, biocide application, membrane surface modification, etc.[17] However, feed pretreatment (such as coagulation or flotation) has limited the application due to high expense [18] and non-persistent effect on bacteria inhibition [19-20]. Continuous application of biocides (e.g., chlorine or ozone) cannot guarantee the inhibition of biofilm formation, but may be detrimental to polymer membranes and generate toxic disinfection byproducts [21-23]. In contrast, surface modification has shown promising performance on the mitigation of membrane fouling [24-26], although it is still challenging to control long-term biofouling [27-30]. Therefore, this study focused on the novel synthetic methods to improve surface hydrophilicity and enhance antibacterial property of membranes.

Recently, blending antibacterial biocidal agents with the membrane backbone materials has been demonstrated as a promising method for the antibacterial modification of membrane [31-32]. Silver is a well-known effective antibacterial agent [33], and its antimicrobial property is size dependent [34]. However, the smaller silver nanoparticles, synthesized by conventional physical and chemical methods, often have problems with particle stability and agglomeration [34-35]. Also, silver is a relatively expensive antibacterial agent, which is a great concern in the engineering application.

Other relatively cheap antibacterial nanoparticles involve nanosized titanium dioxide (TiO_2), silicon dioxide (SiO_2), and zinc oxide (ZnO) [36]. Among them, TiO_2 is the most widely studied material because of its high photocatalytic activity, stability, low cost, and non-toxicity [37-38]. Meanwhile, depending on reactive oxygen species (ROS) produced in the presence of light [39-41], TiO_2 can effectively kill the most of the microorganisms [36].

However, the large band gap of TiO_2 (3.2 eV) seriously limits its utilization under natural sunlight illumination [42].

Ag-n-TiO_2 displays excellent photocatalytic activity, antibacterial property and promising engineering applications. According to the Chinese market quotes, the price of Ag-n-TiO_2 is about 1/20 of nano-Ag particle. Also, as supporting media, TiO_2 can help to disperse the nano-Ag and control the release of the nano-Ag at a proper rate. In addition, the noble metal of Ag has extended the spectral response of TiO_2 into the visible region and improves its photocatalytic performance under visible light [42]. As a result, the Ag-n-TiO_2 can produce ROS more efficiently and its antibacterial property is hence further enhanced [43]. But there is little information about how or whether the antibacterial property of a polymer membrane is improved if modified with Ag-n-TiO_2.

In this study, the influence of Ag-n-TiO_2 on antifouling performance and in-situ antibacterial property of PVC membrane was comprehensively investigated in both short-term *E. coli* adhesion and long-term biofouling testing. The optimal amount of the additive agents was identified for the best membrane performance, and the antibacterial mechanism was revealed in details.

2. Experimental

2.1 Materials

PVC (PSM-31, molecular weight Mw: 80, 000 g/mol) was purchased from Shenyang chemical industry and was dried at 60 ºC in a vacuum oven for 4 h to remove absorbed water. N,N-dimethylacetamide (DMAC, > 99%) (AR, Bodi Co. Ltd., China) was employed as a solvent to prepare casting solution. Polyvinylpyrrolidone (PVP) and polysorbate (T-80) were purchased from Lanji Co. Ltd., China. Polyethyleneglycol (PEG) of different molecular weights ranging from 6, 000 Dalton (Da) to 300,000 Da was purchased from Aladdin Industrial Corporation, China.

2.2 Synthesis and characterization of Ag-n-TiO_2 particles

The precursor of nano-TiO_2 was prepared from industrial H_2TiO_3 and 98% sulfuric acid in continuous acid dissolution and pyro-hydrolysis. It was then embedded with silver in the form of Ag_3PO_4. The total Ag content is controlled at approximately 1.0 wt% on the Ag-n-TiO_2 particles. The microstructures and distributions of the Ag-n-TiO_2 particles were

analyzed by transmission electron microscopy (TEM, JEM-2000EX, Japan) to identify their mean particle size. Before testing, the mixture of 50 mg Ag-n-TiO_2 particles and 50 mL alcohol was sonicated for 30 min at 40 kHz; a drop of the resultant dispersion was deposited and dried on a standard copper grid. The chemical structures of Ag-n-TiO_2 particles were confirmed by a NEXUS 670 Fourier transform infrared spectroscopy (FT-IR, PE-100, USA). FT-IR spectra was collected over 32 scans in the 4000–400 cm^{-1} region by the attenuated total reflection (ATR) mode. Prior to testing, the particles were dried at 60 ºC in a vacuum oven for 4 h to remove the absorbed water.

2.3 Membrane Preparation

2.3.1 Preparation of Ag-n-TiO_2/PVC flat sheet membrane

Phase inversion method was employed to prepare Ag-n-TiO_2/PVC flat sheet membrane. The typical process was as follows: First, the mixture of Ag-n-TiO_2 particles and DMAC was sonicated in a 25 °C ultrasonic bath at 40 kHz for 30 min. Different concentrations of Ag-n-TiO_2, 0.0, 0.5, 1.0, and 1.5 wt% were added, respectively. T-80 (1 wt%), PVP (6 wt%) and PVC (12 wt%) were successively added in to DMAC. Meanwhile, the solutions were stirred at 1200 r/min for 24 h in water bath of 30 °C to acquire a uniform and homogeneous casting solution.

After filtered by a metal screen (40 mesh), these cast solutions were sealed by para-film with reserved holes and stored at 30 °C in a vacuum oven (-0.08 MPa) for 10 h to remove air bubbles. Then the casting solution was casted on a clean glass plate by a stainless-steel knife with a thickness of 500 μm. The glass plate was then exposed in the air of 70% relative humidity for 15 s, and immersed into a coagulation bath (ultrapure water at 25 °C). After complete coagulation, the formed membrane was transferred to another ultrapure water bath, and immersed for 48 h to remove any residual DMAC. Table 1 shows the compositions of each casting solution.

Table 1 Compositions of membrane casting solutions with different Ag-n-TiO_2 loading

Membrane	Ag-n-TiO_2 (wt%)	PVC (wt%)	DMAC (wt%)	PVP (wt%)	T-80 (wt%)
M-0	0	12	81	6	1
M-1	0.5	12	80.5	6	1
M-2	1.0	12	80	6	1
M-3	1.5	12	79.5	6	1

2.3.2 Preparation of Ag-n-TiO_2/PVC reinforced hollow fiber membrane

Ag-n-TiO_2/PVC reinforced hollow fiber membrane and its control sample were fabricated by the dry-jet wet spinning machine. Ag-n-TiO_2 nanoparticles (30 g) were firstly dissolved into DMAC and treated ultrasonically at 40 kHz for 30 min. After the nanoparticle suspension was transferred into the agitator tank, environmental calcium zinc composite of 30 g (W-10, Shandong Wantu Polymer Materials Co., Ltd., China) was added as heat stabilizer. Once the temperature of the agitator tank reaches 65 ºC, PVP, T-80 and pre-dried polymer powder were successively added. The contents were mechanically stirred at 65 ºC for 12 h until a homogeneous dope solution was acquired. This dope solution was degassed in vacuum for overnight ahead of spinning. Details of the spinning procedure and the compositions of the dope solution were described in Fig. S1 and Table S1.

2.4 Membrane Characterization

The surface and the cross-section of the membranes were characterized by a scanning electron microscope (JSM-6480A，JEOL, Japan) at 10 KV in a high vacuum mode after being coated with approximately 10 nm of gold. The flat sheet membranes were first cryogenically fractured under liquid N_2 to expose their cross-sections. In contrast, the cross-sections of the reinforced membranes were directly cut. Elemental analyses of the membranes were carried out using an energy dispersive spectrometer (EDS) equipped with SEM (SEM-EDS).

Atomic force microscope (AFM, Dimension Vx 210/310, Veeco Metrology Group, Japan) was employed to analyze the surface of fabricated flat-sheet membranes. The membrane surfaces were characterized in a scan area of 10 μm × 10 μm, and the surface roughness was acquired by tapping mode. Membrane thickness was characterized by a film

thickness analyzer (CH-1-S, Shanghai Liuling Co., Ltd., China) after the samples were dried at room temperature. Membrane mechanical property was measured by an electric elastic yarn strength analyzer (YG020B, Nantong Sansi Co., Ltd., China). Contact angle (CA) was determined applying 8 different spots on the membrane surface, where each water droplet of 2 μL was carefully placed on the membrane surface and repeated from the same height (about 30 mm). After holding for 5s, the water drop was caught by a computer-controlled camera and then the CA values were automatically collected by JYSP-360 contact angle goniometer (Jin Shengxin Co., Ltd., China). Membrane pure water flux (PWF) was analyzed by dead-end filtration of ultrapure water with a stirred cell unit (Model 8200, Millipore, USA) at 0.1 MPa. Before testing, membrane sample was preload at 0.2 MPa for 10 min.

The membrane porosity (%) was calculated according to the method of dry-wet weight. Mean pore radius was determined by the filtration velocity method as stated in the Guerout-Elford-Ferry equation [44]. Molecular weight cut-off (MWCO) of the membranes was analyzed by measuring the rejection of PEG solutions with different molecular weight. The feeds and permeates were collected and analyzed using a total organic carbon analyzer (TOC-VCPN, Shimadzu Corporation, Japan).

2.5 Antifouling performance and in-situ antibacterial properties analyses

2.5.1 Conventional inhibition zone test

The antibacterial performance of the prepared membrane was investigated by disk diffusion method that employed Gram-negative *Escherichia coli (E. coli)* K12 as model bacteria. Cultures with 1 mL *E. coli* bacteria suspension were incubated at 37 ℃ and shaken at 130 r/min for 12 h. Luri Bertani (LB) agar solid medium were seeded with the bacteria suspension, and then two discs (about 10 mm diameter) of each membrane sample were embedded into the surface layer of the plates, and incubated in a constant temperature incubator at 37 ℃ for another 24 h. Vernier calipers were used to measure the inhibition zones. In order to clarify the effect of light on the antibacterial property of Ag-n-TiO_2 modified PVC membranes, this experiment was performed under both dark and visible light conditions.

2.5.2 *E. coli* adhesion experiment

E. coli was used to investigate bacterial adhesion behavior on the membranes surface

[45]. *E. coli* bacteria suspension was incubated at 37 °C and shaken at 130 r/min until the stationary phase was achieved. After 12 h, the concentration of *E. coli* reached 10^6 cells / mL. Membranes were washed three times with phosphate buffered saline (PBS). The membrane samples were immersed into a 6-well plate filled with 5 mL bacterial suspension, and incubated at 37 °C for 24 h. Bacterial solution was then removed and membranes were washed with PBS three times at 37 °C. All the washing fluid was collected and then 1 mL solution was taken out for further expanded culture on a solid plate culture medium. The shapes of bacteria attached on the sample surfaces were sought by SEM and their three-dimensional structures were further captured by AFM.

2.5.3 Fluorescence stain for living and dead cells

A series of fluorescence stain experiments were carried out to further access the antibacterial properties of Ag-n-TiO_2/PVC membranes, using Hoechst 33342 / propidium iodide kits for charactering the living and dead cells attached on the membranes [46-47]. Specifically, cultures with 1 mL *E. coli* bacteria suspension were incubated at 37 °C and shaken at 130 r/min for 12 h. Then, 100 mL *E. coli* solution was forced to pass through the membrane coupons, and the coupons were washed twice with isotonic saline solution to remove the attached *E. coli* cells. Then the coupons with attached cells were cultured in the isotonic saline solution for 30 min. Further, the attached cells were rinsed for the following dyeing tests with Hoechst 33342 / PI kit. Detailed detection method was described in our earlier work [48].

2.5.4 Long-term continuous biofouling experiment

To access the long-term antibacterial property of the synthesized membrane, the reinforced hollow fiber membranes were placed into membrane modules in continues operation using tap water as the influent and monitored for three months. Long-term continuous biofouling simulator experimental schematic was displayed in Fig. S2. In this experiment, all the pressure of the feed water maintained at 0.1 MPa by adjusting the influent valve, and the average daily permeation fluxes were recorded by measuring the membrane fluxes at different time points. Conventional inhibition zone tests of the fresh modified and unmodified reinforced hollow fiber membranes were performed. At the end of this experiment, the fouled reinforced hollow fiber membranes were extracted, rinsed by pure water and cultured on Luri

Bertani (LB) agar solid medium to examine the residuary bacteria on the membranes' surface. Additionally, the contaminant layers of the fouled membrane surface were analyzed by SEM.

3. Results and discussion

3.1 TEM and FTIR analyses of the Ag-n-TiO_2 particles

TEM images of the Ag-n-TiO_2 particles (Fig. S3 (a)) reveal that the particles exhibit uniform spherical shape, and the average size was around 24.43±0.8 nm. Some smaller particles were also found attached on the Ag-n-TiO_2, which are presumed as the nano-Ag particles, with an average size of 5.41±0.56 nm. The strong absorption peak at 3421 cm^{-1} in the FT-IR spectra (Fig. S3 (b)) corresponds to the stretching vibration absorption of -OH, signifying the excellent hydrophilicities of Ag-n-TiO_2 particles. The peaks at 694 cm^{-1} and 619 cm^{-1} are characteristic peaks of Ti-O bonds.

3.2 Membranes Characterization

Properties of different Ag-n-TiO_2/PVC membranes are shown in Table 2. The membrane thicknesses increased with the Ag-n-TiO_2 loading and reached the maximal value of 538 μm (M-3), which was attributed to the increased viscosities of casting solutions. Table 2 also indicated that CA values evidently decreased with the addition of Ag-n-TiO2 particles. This phenomenon could be attributed to the hydrophilic functional groups such as -OH on the surface of Ag-n-TiO2 particles (Fig. S3 (b)). When they were blended with the PVC resin, Ag-n-TiO2 particles would be uniformly inlaid on the membranes' surface and result in a hydrophilic layer. Therefore, the hydrophilicity of the modified membrane could be improved with addition of Ag-n-TiO2. In addition, the hydrophilicity of the membrane surface was closely related with the porosity. When the inorganic Ag-n-TiO2 particles were dispersed into the organic PVC polymers the addition of nanoparticles to the hydrophobic membrane casting solution, there may form more gaps [49] among the hydrophilic groups on Ag-n-TiO2 and the hydrophobic PVC chains, which appears to help to improve the porosity of the modified membrane (Table 2). The increased porosity of the membrane usually promotes the hydrophilicity.

A significant increase in the pure water flux was observed with the addition of Ag-n-TiO_2 particles. The increased flux can be attributed to the increased porosity and the reduced filtration resistance caused by the enhanced membrane surface hydrophilicity.

Retention capabilities of the modified membranes also present a slightly increase (Table 2), which can be ascribed to the decreased mean pore size.

Table 2 Properties of different Ag-n-TiO_2/PVC membranes

	Thickness (μm)	CA (°)	PWF[a] (LMH)	Porosity (%)	Rejection ratio[b] (%)	Mean pore size (nm)	MWCO (KDa)
M-0	489.8±2.5	79.67±0.75	135±2	68.5	97.49	60.36±0.54	100
M-1	509.0±3.6	61.57±0.25	156±3	77.1	98.16	59.57±0.72	100
M-2	521.0±5.1	57.21±0.33	179±2	84.2	98.41	59.25±0.60	100
M-3	538.0±4.6	54.83±0.34	184±1	86.9	98.67	59.09±0.46	100

[a] The PWF of all the membranes was tested under 0.1 MPa.

[b] The rejection ratio was the PEO with molecular weight of 100 KDa.

Microstructures of the membrane cross-sections and surface (top and bottom) are displayed in Figs. 1 and S4, respectively. Pores of different dimensions were found in both top and bottom surface. As further observed in the cross-section images, all the pores reveal typical asymmetric morphology. Namely, there is a thin and compact filtration layer on the top of the membrane, and a thick and loose supporting layer with a large amount of macro-voids at the bottom. This phenomenon indicates that the addition of Ag-n-TiO_2 particles did not change the asymmetric structures of the membranes' cross-sections. In addition, significant silver and titanium element peaks was observed on the EDS images of modified membranes in contrast with the control sample, which revealed Ag-n-TiO_2 particles have been successfully incorporated. Meanwhile, the intensity of titanium peak was enhanced with the increase of Ag-n-TiO_2 concentration, which indicated that more Ag-n-TiO_2 had been accumulated in the skin layer.

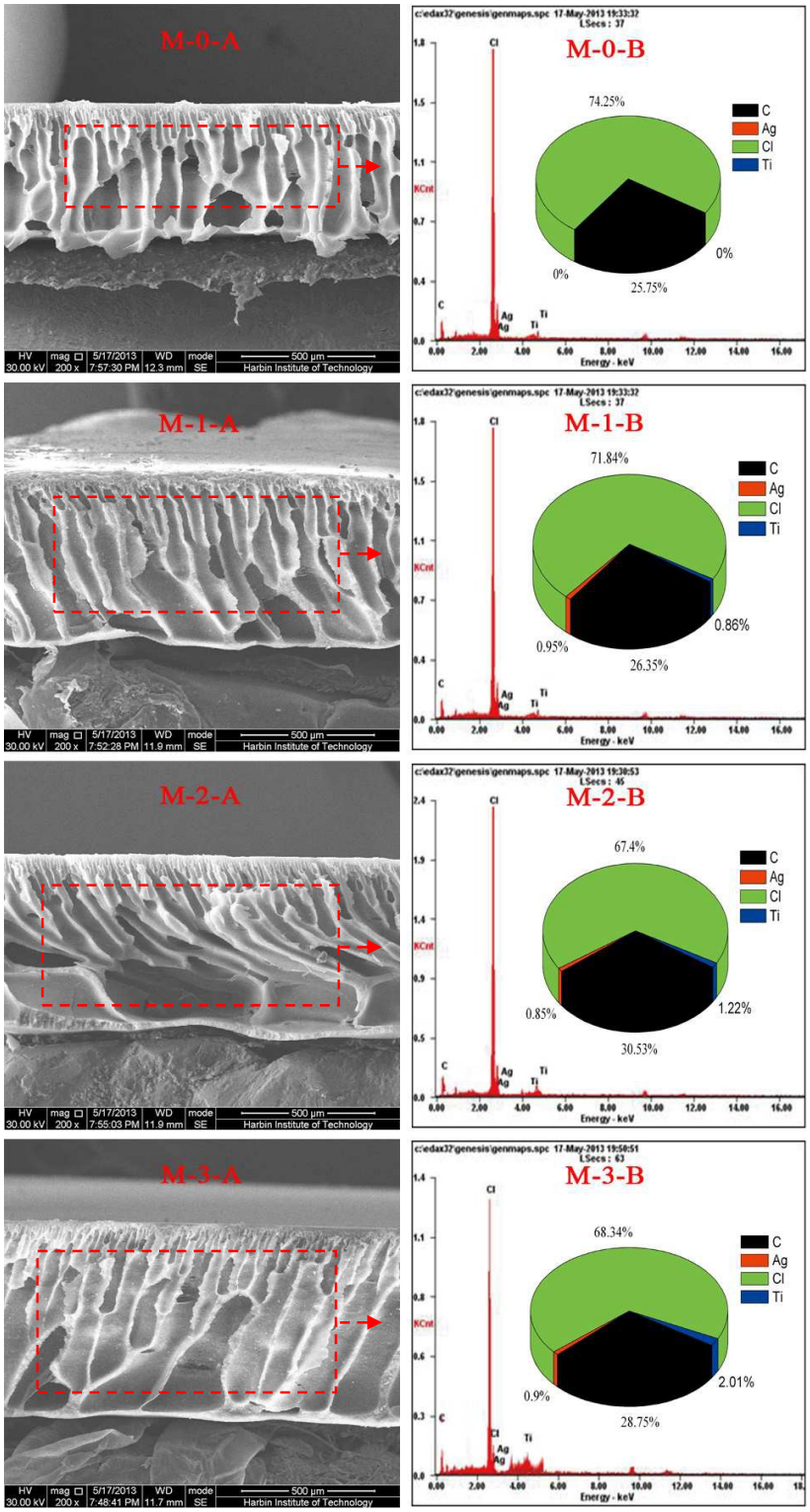

Fig. 1 Cross-section microstructures and EDS images of different Ag-n-TiO_2/PVC membranes

Based on the comprehensive analyses of pure water fluxes, hydrophilicities, retention capabilities, mean pore size, MWCO and microstructures of the different membranes, the

optimum Ag-n-TiO_2 dosage was determined as 1 wt%. Thus, the membrane in the presence of 1.0 wt% Ag-n-TiO_2 was applied as the representative modified membranes for further antibacterial property analyses.

3.4 In-Situ Antibacterial properties analyses in the short-term

3.4.1 Conventional inhibition zone test

Fig. 2 displays that the 1.0 wt% of Ag-n-TiO_2 modified membrane exhibits better antibacterial effect on *E. coli,* since a clear inhibiting ring is found along the outer edge of the membrane disk under both dark and visible light conditions. Meanwhile, the inhibition zone diameter (about 17.78 mm) of the Ag-n-TiO_2 modified membrane under the visible light condition is more significant than that (about 15.56 mm) in dark. The test result indicates the synergetic enhancement in antibacterial property of the Ag-n-TiO_2 modified PVC membranes under the visible light.

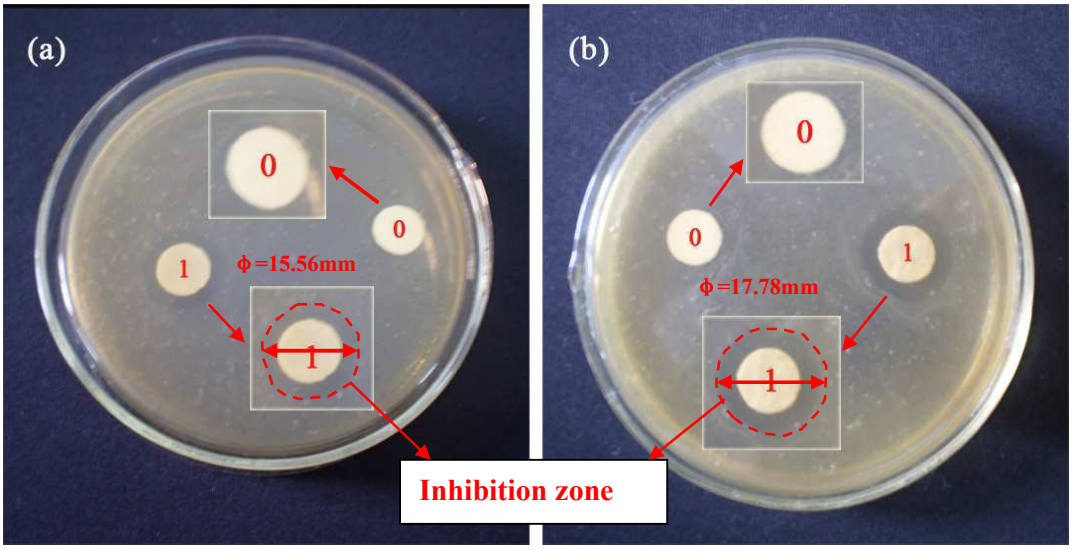

Fig. 2 Inhibition zone of *E. coli* on different Ag-n-TiO_2/PVC membranes (0 is the control membrane sample, 1 is the membrane modified by 1.0 wt% Ag-n-TiO_2) under conditions of dark (a) and visible light (b)

3.4.2 Anti-adhesion effect of *E.coli*

It is obvious that there are fewer *E. coli* attached to the modified membrane (Figs. 3 (a) and (c)) in contrast with the control sample (Figs. 3 (b) and (d)). Only 74 CFU/mL of *E. coli* communities are found in the washing fluid collected from the modified membrane. In contrast, 208 CFU/mL appears in that of the unmodified membrane. These results indicate that the Ag-n-TiO_2/PVC membrane exhibits significant improvement in the anti-adhesion

effect of *E.coli* in the short term. It is also verified by the three-dimensional structures of *E. coli* attached on the membranes' surface. Compared with the unmodified membrane, there exist some damaged cells on the surface of the modified membrane as clearly revealed by AFM images. Generally, damaged cells present worse adhered properties than the living cells.

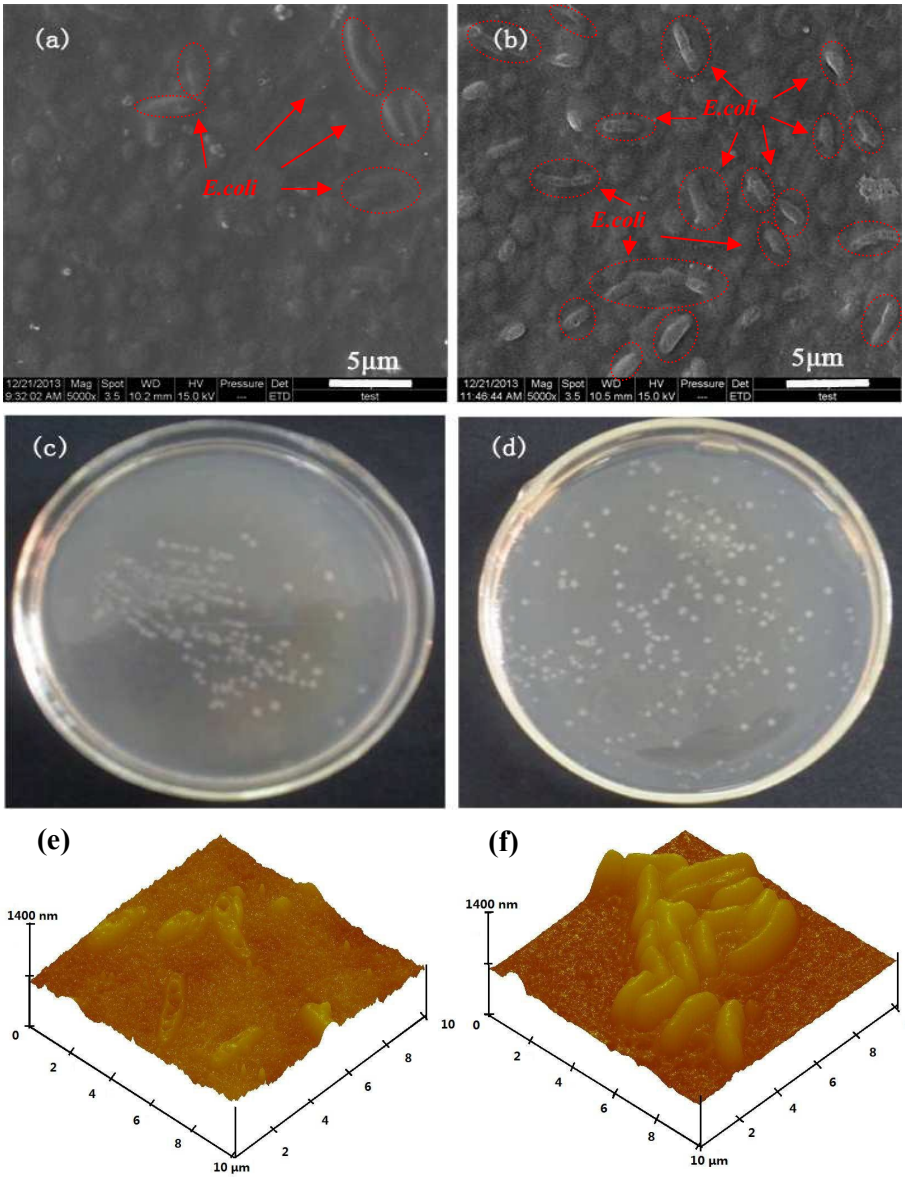

Fig. 3 SEM images of the Ag-n-TiO_2 modified (a) and unmodified membrane surface (b) after *E. coli* attached on, colonies formed on culture by the *E. coli* from the modified (c) and unmodified membrane surface (d), and three-dimensional structures of *E. coli* attached on the surface of the modified membrane (e) and unmodified membrane (f)

3.4.3 Fluorescence stain for living and dead cells

The blue and red regions in fluorescent microscope images (Fig. 4) represent the living cells and dead cells, respectively. It is found that most cells are still living ones (Hoechst 33342 stained) on each sample. Meanwhile, more dead cells (PI stained) are also found on the Ag-n-TiO_2/PVC membrane in contrast with the unmodified membrane. Therefore, Ag-n-TiO_2/PVC membrane shows excellent capability to kill the living cells.

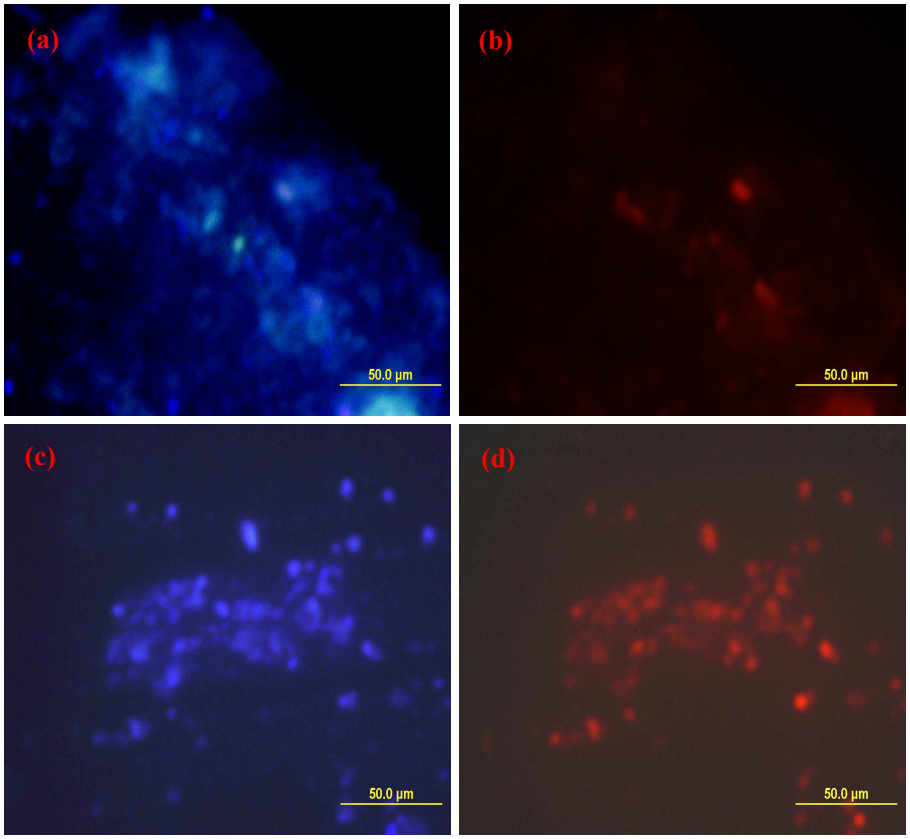

Fig. 4 Fluorescent microscope images of Hoechst 33342/propidium iodide stained cells attached on unmodified membrane ((a) and (b)) and modified membrane ((c) and (d)): PI stained cells (red); Hoechst 33342 stained cells (blue)

3.5 Long-term continuous biofouling analyses

3.5.1 Micro-structures of Ag-n-TiO_2/PVC reinforced hollow fiber membrane

Fig. 5 clearly shows more pores observe on the outer surface of modified membrane than the control sample. There are two clear layers, filtration layer with distinct asymmetric morphology and braidd tube, in the cross-sections (Fig. 5 (c) and (d)). The typical micro-structures exhibit three unique advantages compare with the traditional hollow fiber membrane. First, the braidd tube, as the support of the filtration layer, significantly enhanced

the mechanical property of membrane. The stronger tensile strength makes the membrane endure higher filtration pressure and not easily broken. Thus, this type of membrane has a promising application in drinking water treatment for safety reasons. Secondly, the filtration layer of reinforced membrane can be prepared much thinner than traditional hollow fiber membrane, which helps to further reduce the filtration resistance and leads to a higher flux. Finally, the cheap PVC resin (its price is about 1/10 of PVDF) [50] was chosen as the main matrix of the filter layer, which offsets part of cost brought by the braidd tube.

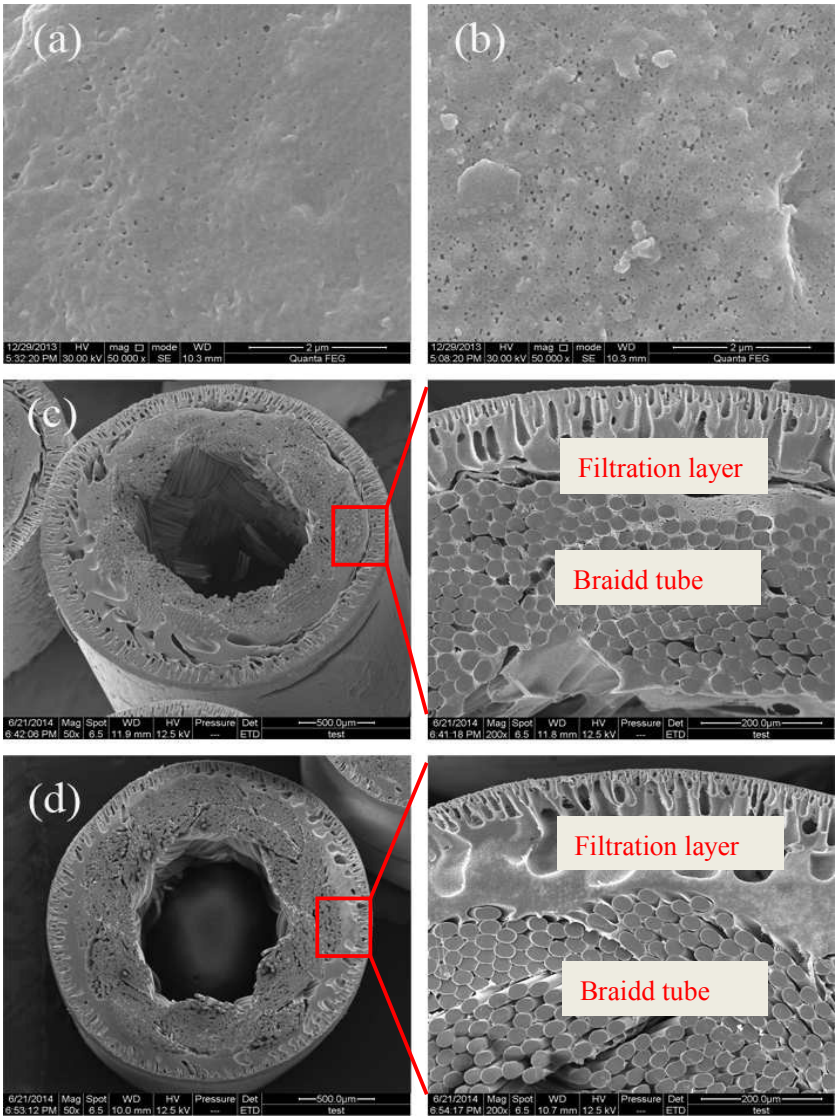

Fig. 5 The SEM images of different Ag-n-TiO_2/PVC hollow fiber membranes: the outer surface images of control sample (a) and modified membrane (b); the cross-setions of control sample (c) and modified membrane (d)

3.5.2 Anti-biofouling performance analysis

The reinforced hollow fiber membrane modified by 1.0 wt% Ag-n-TiO_2 exhibits better antibacterial effect on *E. coli* for the existence of a clear inhibiting zone (Fig. 6(a)). When the fouled hollow fibers were taken from the membrane modules and attached on the culture plates for 24 h, there were some colonies growing on the control sample, while not on the modified one (Fig. 6 (b)). Hence, the Ag-n-TiO_2/PVC modified membrane presents good in-situ antibacterial property to resist the bacteria breeding. In addition, a significant cake layer was observed on the surfaces of both the modified and unmodified membranes (Figs. 6 (c) and (d)). In the long-term filtration process, many contaminants gradually absorbed and accumulated on the membrane surface. Then the contaminants gradually became compact and finally a dense cake layer was formed. This dense cake layer would block most of the membrane pores and further lead to the significant deterioration of permeability. Additionally, there exist more bacteria on the fouled unmodified membrane (Fig. 6 (d)) than on the modified one (Fig. 6 (c)). Also, the cake layer formed on the control sample seems stickier and more compact than the modified membrane. The cake layer may result from the bacteria and their micro-bioproducts such as protein and polysaccharides, etc.

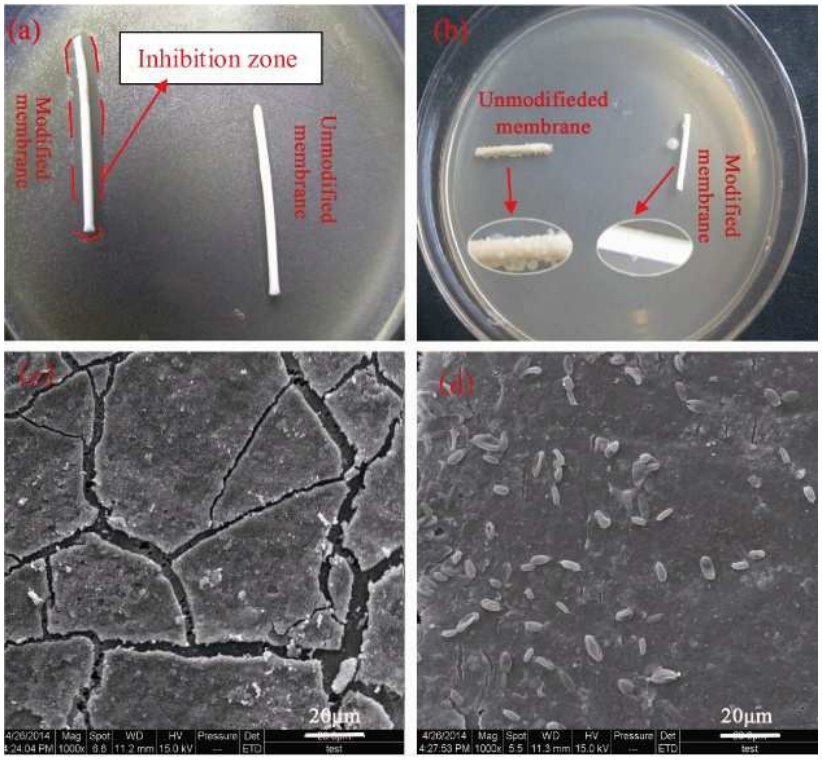

Fig. 6 Inhibition zone of *E. coli* on different hollow fiber membranes (a), the bacterial colonies on the fouled hollow fiber membranes (b), SEM images of the fouled Ag-n-TiO_2/PVC hollow fiber membrane (c) and unmodified hollow fiber membrane (d)

3.5.3 Permeation fluxes and flux recovery analyses

Fig. S5 (a) shows that both the modified and the unmodified membranes present a decrease in the permeation fluxes during three months of filtration. However, the decreased trend of the modified membrane is much slower than the control sample, especially at the beginning of the continuous filtration process (0-20 days). This could be attributed to the better hydrophilicity and antibacterial property of the Ag-n-TiO_2/PVC membrane. However, the advantage of modified membrane was not significant after the formation of a dense cake layer on the membrane surface in the long-term filtration process (Fig. 6 (c)). Hence, the flux of the modified membrane also presents a gradual decline in the 60-90 days.

Flux recovery ratios (FRR) after washing with different kinds of cleaning solution were displayed in Fig. S5 (b). The modified membrane presents better antifouling performance for the higher FRR values. In addition, the FRR values washed with pure water were rather low for unmodified membrane (40.5%) and modified membranes (51.3%), while the value of washed with 12% NaClO solutions for modified membrane were about 80%, which indicates that most membrane fouling formed in the process of long-term filtration is not reversible fouling but the biofouling.

3.5.4 Retention ability analysis

The water quality summarized in Table S2 show that this novel reinforced hollow fiber membrane presents outstanding performance for water purification. For its smaller pore size, the membranes modified by Ag-n-TiO_2 particles exhibited higher retention properties for the UV_{254}, residual iron, and NH_4^+-N than the unmodified membrane at the beginning of the filtration. However, the unmodified membrane presents better retention ability after three months continuous filtration. The reason is that the membrane was fouled for the deposits of the foulant and the fouled cake layer acted as a second filtration layer (as shown in Fig. 6) to increase the membrane filtration resistance. Because of the enhanced hydrophilicity and antibacterial performance, the formation of the fouled cake layer on modified membrane was delayed. Even if the pollution layer was formed, it is relatively loose because of the weaker

microbial metabolic activity. In addition, this novel UF membrane can effectively remove the bacteria due to its reasonable pore size, which is helpful to the following disinfection process.

3.6 In-Situ Antibacterial mechanism analysis

The excellent antibacterial property both in short-term and long-term of the Ag-n-TiO_2 modified membrane can be attributed to its novel structure. As shown in Fig. 7, Ag-n-TiO_2 particles added into the PVC casting solutions can be uniformly inlaid on the membrane's surface and pores. Firstly, there exist abundant -OH groups on the surface of Ag-n-TiO_2 particles (Fig. S3 (b)). It is proposed that they can interact with Cl atoms of PVC chains through hydrogen bonds and form a hydrophilic layer on the membrane surface. Generally, the outer cell-wall of the bacterium consists of the fat-like or protein–like substances which are prone to attach on the hydrophobic surface [50]. In addition, the hydrophobic surface tends not to be wetting by water. Once the attachment happens, it is not easily removed by hydraulic washing. On the contrary, the hydrophilic membrane surface helps to resist initial formation of the biofilm [28]. Secondly, AFM analysis showed that addition of Ag-n-TiO_2 can decrease the mean roughness (R_{ms}) of the modified PVC compared with control membrane (Table S3). The rougher surface topography is generally more readily to cause the bacterial attachment. Specifically, a greater roughness can increase the total surface area (Table S3) and the ridge–valley structure (Fig. S6), which leads to accumulation of foulants including bacteria and their micro-bioproducts. As a result, membranes with rougher surfaces are more favorable for the attachment of bacteria and other foulants, leading to faster fouling rates [51-52].

More significantly, the releases of Ag^+ and ROS from Ag-n-TiO_2 particles inlaid on the membrane do great contribution to the antibacterial property of the modified membrane. The excellent antibacterial property is closely related with the outer conditions. Specifically, the release of dissolved silver ions especially contributes to keep the membrane antibacterial property under dark condition (Fig. 2 (a)). Actually, nano-Ag particles have the antimicrobial efficacy by their ability to release silver ions, which has a strong antibacterial activity against many kinds of bacteria even at lower concentrations [53]. Under visual light, the photo-induced electrons can transfer to and be trapped by the Ag particles loaded on the surface of TiO_2 effectively (Fig. S7). Accordingly, more separated photo-induced electrons

and holes can be produced, resulting in more oxidizing peroxy or superoxy species to participate photocatalytic degradation reaction [42, 54-55]. It is proposed that the ROS can not only kill the bacteria and virus, but also decompose the micro-bioproducts more effectively (Fig. 7). This assumption can be further verified by the completely damaged bacteria structures on the surface of the modified membrane under visual light (Fig. 3 (e)). In particular, TiO_2, as the carriers of nano-Ag, can control the release rate of nano-Ag and help to keep the long-term antibacterial property (Fig. S8).

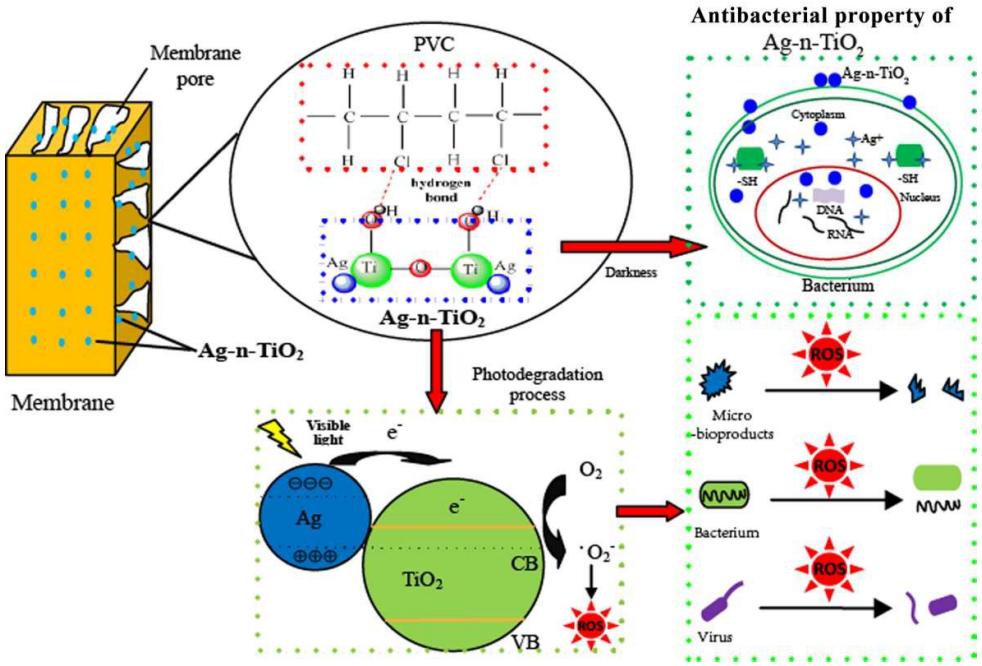

Fig. 7 Schematic illustration of the antibacterial property of Ag-n-TiO_2/PVC membrane

4. Conclusions

In this study, Ag-n-TiO_2 particles were synthesized and utilized as the biocidal agents to modify the PVC membranes. The major contribution of this investigation can be concluded as follows:

(1) With appropriate Ag-n-TiO_2 addition, the hydrophilicity, retention capability, and permeability of PVC-based membrane were significantly enhanced.

(2) For modified membranes with variety of loading rates (0~1.5 wt%), the membrane modified with 1.0 wt% Ag-n-TiO_2 presented the best in-situ antibacterial property in the short-term *E. coli* adhesion.

(3) The Ag-n-TiO_2/PVC membrane module presented significant enhancement in the permeation fluxes, flux recovery ratio, and anti-biofouling performance in the 3 months

long-term filtration experiments. Morphology analyses of the fouling layers revealed excellent antibacterial property of the modified membrane, which could be attributed to the releases of Ag^+ and ROS from Ag-n-TiO_2 particles.

(4) In-situ antibacterial mechanism analysis revealed that the higher hydrophilicity, lower roughness, and better antibacterial property of the membrane were responsible for its significant improvement in the performance against biofouling. Thus, the Ag-n-TiO_2/PVC membrane shows its promising potential in the application of the industrial UF separation process.

Acknowledgements

This work was supported by the National Natural Science Foundation of China (51108112), the Natural Science Foundation of Heilongjiang Province (E201252), Project of Applicable Technology Research and Development of Harbin City (2013DB4BG010), and Open Project of State Key Laboratory of Urban Water Resource and Environment, Harbin Institute of Technology (ESK201004).

References

[1] R. Jamshidi Gohari, E. Halakoo, W.J. Lau, M.A. Kassim, T. Matsuura, A.F. Ismail, RSC Adv., 2014, 4,17587-17596.

[2] A. Cassano, C. Conidi, E. Drioli, Water Res., 2011, 45, 3197-3204.

[3] M. Kumar, D. McGlade, J. Lawler, RSC Adv., 2014, 4, 21699-21711.

[4] H. Yamamura, K. Kimmura, Y. Watabab, Environ. Sci. Technol., 2007, 41,6789–6794.

[5] H. Susanto, M. Ulbricht, Water Res., 200, 42, 2827–2835.

[6] S.R.H. Abadi, M.R. Sebzari, M. Hemati, F. Rekabdar, T. Mohammadi, Desalination, 2011, 265, 222-228.

[7] J.R. Pan, Y.C. Su, C. Huang, H.C. Lee, J. Membr. Sci., 2010, 349, 287-294.

[8] F. Meng, S.-R. Chae, A. Drews, M. Kraume, H.-S. Shin, F. Yang, Water Res., 2009, 43, 1489-1512.

[9] W. Guo, H.-H. Ngo, J. Li, Bioresour. Technol., 2012, 122, 27-34.

[10] W. Gao, H. Liang, J. Ma, M. Han, Z.-l. Chen, Z.-s. Han, G.-b. Li, Desalination, 2011, 272, 1-8.

[11] M. Pasmore, P. Todd, S. Smith, D. Baker, J. Silverstein, D. Coons, C.N. Bowman, J. Membr. Sci., 2001, 194, 15-32.
[12] L. Malaeb, P. Le-Clech, J.S. Vrouwenvelder, G.M. Ayoub, P.E. Saikaly, Water Res., 2013, 47, 5447-5463.
[13] J.S. Baker, L.Y. Dudley, Desalination, 1998, 118, 81-89.
[14] R. Malaisamy, D. Berry, D. Holder, L. Raskin, L. Lepak , K.L. Jones, J. Membr. Sci., 2010, 350, 361-370.
[15] M.S. Maute, M. Elimelech, Environ. Sci. Technol., 2008, 16, 5843–5859.
[16] M. Herzberg, S. Kang, M. Elimelech, Environ. Sci. Technol., 2009, 43, 4393–4398.
[17] J. Yu, G.-A. Shin, B.S. Oh, J.-I. Kye, J. Yoon, Desalination, 2015, 357, 1-7.
[18] V. Kochkodan, N. Hilal, Desalination, 2015, 356, 187-207.
[19] H.C. Flemming, G. Schaule, T. Griebe, J. Schmitt, A. Tamachkiarowa, Desalination, , 113, 215-225.
[20] L.A. Bereschenko, H. Prummel, G.J.W. Euverink, A.J.M. Stams, M.C.M. van Loosdrecht, Water Res., 2011, 45, 405-416.
[21] C. Yu, J. Wu, A.E. Contreras, Q. Li, J. Membr. Sci., 2012, 423–424,487-494.
[22] D. Kim, S. Jung, J. Sohn, H. Kim, S. Lee, Desalination, 2009, 238, 43-52.
[23] H. Xu, W. Chen, H. Xiao, X. Hu, Desalination, 2014, 336, 187-195.
[24] H.Y., Yu, Y.J. Xie, M.X. Hu, J.L. Wang, S.Y. Wang, Z.K. Xu, J. Membr. Sci., 2005, 254, 219-227.
[25] M.P. González Muñoz, R. Navarro, I. Saucedo, M. Avila, P. Prádanos, L. Palacio, F. Martínez, A. Martín, A. Hernández, Desalination, 2006, 191, 273-278.
[26] D. Rana, T. Matsuura, Chem. Rev., 2010, 4, 2448–2471.
[27] D.J. Miller, P.A. Araújo, P.B. Correia, M.M. Ramsey, J.C. Kruithof, M.C.M. Van Loosdrecht, B.D. Freeman, D.R. Paul, M. Whiteley, J.S. Vrouwenvelder, Water Res., 2012, 46, 3737-3753.
[28] W. Lee, C.H. Ahn, S. Hong, S. Kim, S. Lee, Y. Baek, J. Yoon, J. Membr. Sci., 2010, 351, 112-122.
[29] Y. Baek, J. Yu, S.-H. Kim, S. Lee, J. Yoon, J. Membr. Sci., 2011, 382, 91-99.
[30] J. Pieracci, J.V. Crivello, G. Belfort, J. Membr. Sci., 1999, 156, 223-240.

[31]J. Huang, H. Wang, K. Zhang, Desalination, 2014, 33, 8-17.

[32]M. S. Mauter, Y. Wang, K. C. Okemgbo, C. O. Osuji, E. P. Giannelis, M. Elimelech, ACS Appl. Mater. Interfaces, 2011, 3, 2861–2868

[33]D. Huo, J. Gao, B. Guo, Y. Ding, J. He, H. Yu, Z. Zhou, Y. Hu, Rsc Adv., 2013, 3, 10632-10638.

[34]G.A. Martínez-Castanón, N. Nino-Martínez, F. Martínez-Gutierrez, J.R. Martínez-Mendoza, F. Ruiz, J. Nanopart. Res., 2008, 10, 1343-1348.

[35]S. Agnihotri, S. Mukherji, S. Mukherji, Rsc Adv, 2014, 4, 3974-3983.

[36]L.K. Adams, D.Y. Lyon, P.J.J. Alvarez, Water Res., 2006, 40, 3527-3532.

[37]A. Fujishima, K. Honda, Nature, 1972, 238, 37-38.

[38]J. Matos, M. Hofman, R. Pietrzak, Carbon, 2013, 54, 460-471.

[39]M. Cristina Yeber, J. Rodríguez, J. Freer, N. Durán, H. D. Mansilla, Chemosphere, 2000, 41, 1193-1197.

[40]B. Fubini, A. Hubbard, Free Radical Biol. Med., 2003, 34, 1507-1516.

[41]M. Kubo, R. Onodera, N. Shibasaki-Kitakawa, K. Tsumoto, T. Yonemoto, Biotechnol. Progr., 2005, 21, 897-901.

[42]L. Liang, Y. Meng, L. Shi, J. Ma, J. Sun, Superlattices Microstruct., 2014, 73, 60-70.

[43]N.H. Ahmad Barudin, S. Sreekantan, M.T. Ong, C.W. Lai, Food Control, 2014, 46, 480-487.

[44]H. Basri, A.F. Ismail, M. Aziz, Desalination, 2011, 273, 72-80.

[45]A. Venault, Y.-H. Liu, J.-R. Wu, H.-S. Yang, Y. Chang, J.-Y. Lai, P. Aimar, J. Membr. Sci., 2014, 450, 340-350.

[46]S. Kang, S.M. Mauter, M. Elimelech, Environ. Sci. Technol., 2008, 42, 7528–7534.

[47]S. Kang, M. Pinault, L.D. Pfefferle, M. Elimelech, Langmuir, 2007, 23, 8670–8673.

[48]Z. Fangbo, Q. Feng, Z. Xiaohui, Y. Shuili, K. Han-Shin, P. Hee-Deung, T. Satoshi, W. Peng, Water Sci. Technol., 2012, 66, 2275-2283.

[49]J.-n. Shen, H.-m. Ruan, L.-g. Wu, C.-j. Gao, Chem. Eng. J., 2011, 168, 1272-1278.

[50]Z. J. Yu, X. Y. Liu, F. B. Zhao, X. Y. Liang and Y. Tian, J. Appl. Polym. Sci., 2015, DOI: 10.1002/app.41267.

[51]S.J. Oh, N. Kim, Y.T. Lee, J. Membr. Sci., 2009, 345, 13-20.

[52]E.M. Vrijenhoek, S. Hong, M. Elimelech, J. Membr. Sci., 2001, 188, 115-128.

[53]Q. Cheng, C. Li, V. Pavlinek, P. Saha, H. Wang, Appl. Surf. Sci., 2006, 252, 4154-4160.

[54]H.M. Sung-Suh, J.R. Choi, H.J. Hah, S.M. Koo, Y.C. Bae, J. Photochem. Photobiol., A, 2004, 163, 37-44.

[55]M. Jakob, H. Levanon, P.V. Kamat, Nano Lett., 2003, 3, 353-358.